Journal of Power Sources 196 (2011) 8948–8954

Contents lists available at ScienceDirect

Journal of Power Sources

journal homepage: www.elsevier.com/locate/jpowsour

Response of a planar solid oxide fuel cell to step load and inlet flow temperature changes

Pejman Kazempoor[a,b,*], Fathollah Ommi[a], Viktor Dorer[b]

[a] Department of Mechanical Engineering, Tarbiat Modares University, Tehran, Iran
[b] Empa, Swiss Federal Laboratories for Materials Science and Technology, Building Science and Technology Laboratory, CH-8600 Dübendorf, Switzerland

ARTICLE INFO

Article history:
Received 18 November 2010
Received in revised form 13 January 2011
Accepted 13 January 2011
Available online 26 January 2011

Keywords:
Solid oxide fuel cell
Planar cell geometry
Step load change
Dynamic behaviour
Mathematical simulation

ABSTRACT

To explore the dynamic characteristics of the SOFC systems and to develop relevant control strategies, a previously developed steady state SOFC model is converted to a dynamic model. The model includes mass, momentum, thermal and electrochemical analysis, as well as the kinetic model of hydrocarbon reactions. Applying two control strategies i.e., cell constant fuel flow rate and constant fuel utilization during the transient time, the model is implemented to analyse the dynamic behaviour of a planar direct internal reforming (DIR) SOFC cell under several step-load changes. Transient response, resulting from an inlet temperature variation, is also investigated. The results show that the relaxation time is strongly related to the thermal behaviour of the cell and the applied control strategy. However, it is almost independent of the load variation magnitude.

1. Introduction

With the advantages of its high efficiency, high reaction kinetics, high power density, fuel flexibility and, as well as high level of usable heat; the high temperature solid oxide fuel cell (SOFC) is identified as one of the most promising technologies for future power generation in both large central power station plants and distributed power generation stations. However, the SOFC technology faces many challenges when it comes to commercialization, since cost reductions, increasing the reliability of components and extended durability are required. To overcome these challenges, one needs to understand the complex operating mechanism of the SOFC stack, such as heat and mass transfer, together with electrochemical reactions. Under steady-state operation, the high temperature and aggressive environment inside the SOFC stack, as well as the failure of fuel cell system components, can cause harmful conditions on the SOFC stack. In addition to steady state operation, as the demand for electrical power is frequently fluctuating, the technology also has to remain reliable and stable with transient situations such as start-up, shut-down and load change. Therefore, it is increasingly important to understand the fundamental mechanisms and SOFC behaviours under transient operating conditions. Furthermore, knowledge about the SOFC dynamic behaviour can be employed to design a control scheme for the SOFC operation and to compensate its dynamic interactions with the rest of the system.

As the experimental investigations on SOFCs are time-consuming and expensive, mathematical modelling techniques have been proved to be a cost effective method to investigate both steady state and transient behaviour of SOFCs. There are many examples of modelling investigations in literature. Most models, however, are in steady state condition [1–5] and transient SOFC models, typically, are not as elaborate as steady-state models. Achenbach presented one of the first transient studies on SOFCs [6]. He considered a three-dimensional and time-dependent mathematical model of a planar SOFC, together with semi empirical voltage polarization equations. Ota et al. [7] investigated the dynamic behaviour of a micro-tube SOFC. A dynamic model for tubular SOFC developed by Sedghisigarchi and Feliachi [8] based on the lumped capacitance model. Aguiar et al. [9] presented the open and closed-loop transient response of a co-flow planar anode-supported intermediate-temperature (IT) direct internal reforming (DIR) solid oxide fuel cell to load step changes. A reduced 1D dynamic model of a planar DIR-SOFC, with assumption of uniform current density distribution and one temperature layer, for system research is introduced by Kang et al. [10]. A thorough review of the state-of-the-art in dynamic modelling is presented in [11,12].

The overall aim of the present study is to evaluate the performance of a planar SOFC system for residential applications in both steady state and transient conditions. Results of the cell and system

* Corresponding author at: Department of Mechanical Engineering, Tarbiat Modares University, Tehran, Iran, P.O.B. 1415111. Tel.: +98 21 82884397; fax: +98 21 82884922.
E-mail addresses: p_kazempoor@modares.ac.ir, pejman.kazempoor@empa.ch, pejmankazempoor@gmail.com (P. Kazempoor).

0378-7753/$ – see front matter © 2011 Elsevier B.V. All rights reserved.
doi:10.1016/j.jpowsour.2011.01.047

Nomenclature

Latin letters

A	area (m^2)
AER	excess air flow ratio
C_i	molar concentration of component i ($mol\,m^{-3}$)
CP	specific heat ($kJ\,kg^{-1}\,K^{-1}$)
E_{Nernst}	Nernst cell potential (V)
$\dot{E}$	rate of energy flow ($kJ\,s^{-1}$)
$\dot{E}_{Proud,\,i}$	rate of energy transfer accompanying mass transfer of product i ($kJ\,s^{-1}$)
$\dot{E}_{react,\,i}$	rate of energy transfer accompanying mass transfer of reactant i ($kJ\,s^{-1}$)
FU	fuel utilization (%)
H	hight (m)
i	cell current (A)
i_0	exchange current (A)
J	current density ($A\,m^{-2}$)
LHV	lower heating value ($J\,mol^{-1}$)
$\dot{n}$	molar flow rate ($mol\,s^{-1}$)
$\dot{n}_{f,\,consumed}$	fuel consumed in each channel ($mol\,s^{-1}$)
P_{DC}	stack DC power output (W)
q	heat flux ($kW\,m^{-2}$)
$\dot{r}_j$	rate of reaction j ($mol\,m^{-2}\,s^{-1}$)
T	temperature (K)
t	time (s)
V_{op}	cell voltage (V)
V	volume of a computational element (m^3)
x	axial coordinate (m)

Greek symbols

η_{act}	activation polarization (V)
η_{cell}	cell-stack efficiency
η_{dif}	diffusion polarization (V)
η_{ohm}	ohmic polarization (V)
ν_{ij}	stoichiometric coefficient of component i in reaction j
ρ	density ($kg\,m^{-3}$)
τ	relaxation time (s)

Superscripts

cond	conduction
conv	convection
Rad	radiation

Subscripts

A	air
An	anode
ave	average
Ca	cathode
El	electrolyte
F	fuel
Final	final condition after variable change (new steady state condition)
Initial	initial condition before variable change (old steady state condition)
IcA	air side interconnector
IcF	fuel side interconnector
In	inlet
Nernst	Nernst potential
ohm	ohmic
out	outlet
Ox	oxidation reaction
PEN	positive-electrode/electrolyte/negative electrode
red	reduction reaction
SR	steam reforming reaction
WGS	water gas shift reaction

models in steady state condition have been previously published in [13,14]. In this article, as an incremental step toward a more comprehensive understanding of the dynamic behaviour of planar DIR-SOFC systems, a previously developed steady state SOFC cell model is converted to a dynamic model. By using this model, the SOFC dynamic behaviour is investigated based on two strategies i.e., constant flow rates to the system and constant fuel utilization during the cell transient operation. Transient response, resulting from an inlet temperature variation, is also investigated.

2. SOFC cell and stack model description

Only a brief description of the cell models applied is given here (for details see [13,14]).

The considered SOFC configuration is a planar type in both anode-supported (or intermediate temperature (IT)) and electrolyte-supported (or high temperature (HT)) designs (Fig. 1). A general detailed quasi 2D model based on the mass, momentum, thermal and complete electrochemical analysis, as well as the kinetic model of hydrocarbon reactions, is developed for the considered geometry. The planar SOFC cell is divided into a series of piped-type volumes (unit elements) and the finite volume method is used to discretize the governing equations on each unit element. The main assumptions of the cell model are [13]:

(1) One-dimensional cell representation along the streamwise direction.
(2) Uniform distribution of feed gases to each channel.
(3) Each of the gas channels in the unit cell act as continuously stirred tank reactors (CSTR).
(4) Lumped temperature of the solid cell structure (anode–electrolyte–cathode).
(5) Adiabatic boundaries at the cell inlet and outlet.

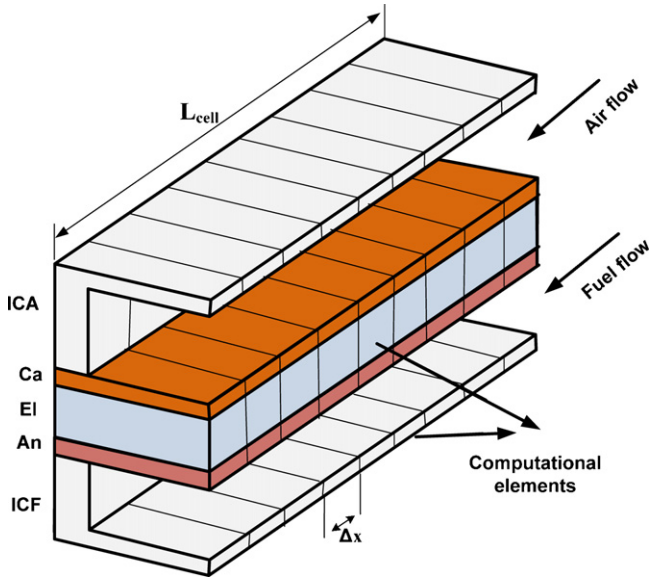

Fig. 1. Planar SOFC geometry.

Due to the high electrical conduction, electrodes and current collector act as isopotential surfaces.

The electrochemical analysis comprises the complete evaluation of the cell ohmic, activation and concentration polarizations. These polarizations are subtracted from the Nernst potential to calculate the unit element operational voltage:

$$V_{Op} = E_{Nernest} - (\eta_{ohm} + \eta_{act,\,Ca} + \eta_{act,\,An} + \eta_{diff,\,Ca} + \eta_{diff,\,An}) \quad (1)$$

For calculation of the ohmic polarization, equivalent ohmic resistance is calculated for each unit element by dividing it into several parts. Ohm's law is then applied to calculate the ohmic losses. As the reactant gaseous concentrations in the triple phase boundary (TPB) are needed to calculate the concentration polarization, two levels of diffusion phenomena, between the bulk gas phase to the electrode surface, and between electrode surface and triple phase boundary are considered. The Fick's model is then applied to calculate the reactant gaseous concentrations in the electrode surface and TPB, respectively. The Fuller equation is used to calculate the binary diffusion coefficients. The Knudsen diffusion coefficients are calculated based on the average molecular speed of each component. The effective diffusion coefficients are also calculated based on the binary and Knudsen diffusion coefficients with consideration to the mixing rule.

The complete form of the Butler–Volmer equation, with selective transfer coefficient (two step equation [15]), is also applied to calculate the activation polarization.

The continuity equations comprise the anode and cathode molar flow rate variations due to the, internal reforming of methane, and water–gas-shift reactions:

$$\frac{d(C_i)}{dt} = -\frac{d\dot{n}_i}{dx} + \sum_{j=WGS,\,SR,\,Ox} \nu_{ij}\dot{r}_j \quad i \in \{CH_4,\ CO_2,\ CO,\ H_2O,\ H_2,\ N_2\} \quad \text{anode} \quad (2)$$

$$\frac{d(C_i)}{dt} = -\frac{d\dot{n}_i}{dx} + \sum_{j=red} \nu_{ij}\dot{r}_j \quad i \in \{O_2,\ N_2\} \quad \text{cathode} \quad (3)$$

As described in [13], to improve the accuracy of the thermal model, five layers of temperatures are considered in energy balance equations. Radiation between solid parts is also considered in the thermal model. Therefore, for each unit element, the energy balance equations are written for the fuel and air side, PEN (positive electrode–electrolyte–negative electrode), and air and fuel streams as:

$$\rho_{F,\,ave} V_F CP_{F,\,ave} \frac{dT_F}{dt} = \dot{E}_{in,\,F} - \dot{E}_{out,\,F} + q^{conv}_{PEN,\,F} A_{conv} + q^{cond}_{IcF,\,IcA} A_{cond} - \dot{E}_{React,\,H_2} + \dot{E}_{Proud,\,H_2O} \quad \text{Fuel flow} \quad (4)$$

$$\rho_{A,\,ave} V_A CP_{A,\,ave} \frac{dT_A}{dt} = \dot{E}_{in,\,A} - \dot{E}_{out,\,A} + q^{conv}_{PEN,\,A} A_{conv} + q^{cond}_{IcF,\,IcA} A_{cond} - \dot{E}_{React,\,O_2} \quad \text{Air flow} \quad (5)$$

$$\rho_{PEN,\,ave} V_{PEN} CP_{PEN,\,ave} \frac{dT_{PEN}}{dt} = q^{cond}_{PEN} A_{cond} - q^{conv}_{PEN,\,F} A_{conv} - q^{conv}_{PEN,\,A} A_{conv} + q^{Rad}_{PEN,\,IcA} A_{Rad} + q^{Rad}_{PEN,\,IcF} A_{Rad} + \dot{E}_{React,\,H_2} + \dot{E}_{React,\,O_2} - \dot{E}_{Produ,\,H_2O} - iV_{op} \quad \text{PEN} \quad (6)$$

$$\rho_{IcA,\,ave} V_{IcA} CP_{IcA,\,ave} \frac{dT_{IcA}}{dt} = q^{cond}_{IcA} A_{cond} - q^{conv}_{IcA,\,A} A_{conv} - q^{Rad}_{PEN,\,IcA} A_{Rad} \quad \text{Air side interconnect} \quad (7)$$

$$\rho_{IcF,\,ave} V_{IcF} CP_{IcF,\,ave} \frac{dT_{IcF}}{dt} = q^{cond}_{IcF} A_{cond} - q^{conv}_{IcF,\,F} A_{cond} - q^{Rad}_{PEN,\,IcF} A_{Rad} \quad \text{Fuel side interconnect} \quad (8)$$

In the model, the fully developed laminar flow solutions of the Navier–Stokes equations or steady Hagen–Poiseuille analysis, is used for calculation of the pressure losses inside the air and fuel channels [16]. The enthalpy of the mixtures in the flow channels are evaluated by the molar mixing law. The kinetic theory of gases is used to calculate the dynamic viscosity and thermal conductivity of the mixtures.

For discretization of the spatial and temporal terms in the applied equations, the implicit upwind and second order central scheme are utilized, respectively.

3. Model parameters

SOFC fuel utilization (FU), air excess ratio (AER) and efficiency respectively are defined as:

$$UF = \frac{\dot{n}_{f,\,consumed}}{(4\dot{n}_{CH_4} + \dot{n}_{CO} + \dot{n}_{H_2})_{An,\,In}} \quad (9)$$

$$AER = \frac{(\dot{n}_{O_2})_{Ca,\,in}}{[2\dot{n}_{CH_4} + 0.5(\dot{n}_{CO} + \dot{n}_{H_2})]_{An,\,In}} \quad (10)$$

$$\eta_{Cell} = \frac{P_{DC}}{(\dot{n}_F\,LHV_f)_{An,\,In}} \quad (11)$$

Relaxation time (τ) is also an important parameter in investigating the dynamic behaviour of fuel cells. It is defined as the period necessary to recover a percentage (usually 90%, 95% or even 99%) of the dynamic voltage drop (or increase) resulting from the difference $\Delta V = V(t \to \infty) - V(t = +0)$ [6], where the $t = +0$ term shows a very short time after the load change.

4. Results

This section is divided into two sub-sections. Section 4.1 gives results of the cell transient responses to several load changes, for different control strategies (first strategy: example Cases 1 and 2, second strategy: Case 3). Section 4.2 gives results of the cell transient responses to an inlet flow temperature change (Case 4).

A co-flow planar electrolyte-supported DIR-SOFC is selected for the present study. The input parameters of the model are shown in Table 1. As can be seen, methane with 30% pre-reforming is considered as input fuel composition to the model. During the load and temperature changes, the AER parameter is fixed to a constant value. It does not necessarily mean that the air flow rate is completely constant. Based on Eq. (10), in a constant AER, the air flow rate is dependent on the fuel flow rate to the cell.

4.1. Transient response to step-load changes

In this study, the transient behaviour of a planar DIR-SOFC is investigated under two control strategies. In the first strategy, it is assumed that the fuel and air flow rates are constant after the average current density step-change (or step-load change). As a result, the FU parameter changes to a new value which is proportional to the new average current density. Therefore, in a positive load

Table 1
SOFC model input parameters.

Geometry	
Anode thickness/m	50×10^{-6}
Cathode thickness/m	50×10^{-6}
Electrolyte thickness/m	150×10^{-6}
Interconnector thickness/m	2.5×10^{-3}
Cell active area (width × height)/mm^2	100×100
Channel height, fuel side/m	1×10^{-3}
Channel height, air side/m	1×10^{-3}
Channel width, fuel side/m	3×10^{-3}
Channel width, air side/m	3×10^{-3}
Number of channels, fuel side	18
Number of channels, air side	18
Material electrical properties	
Conductivity of anode/W m^{-1} K^{-1}	2.0
Conductivity of cathode/W m^{-1} K^{-1}	2.0
Conductivity of interconnector/W m^{-1} K^{-1}	2.0
Interconnector specific resistivity/Ω m	$\frac{9.30\times10^6}{T_{In}} \exp\left(\frac{-1100}{T_{In}}\right)$
Cathode specific resistivity/Ω m	$\frac{42.0\times10^6}{T_{PEN}} \exp\left(\frac{-1200}{T_{PEN}}\right)$
Electrolyte specific resistivity/Ω m	$3.34 \times 10^4 \exp\left(\frac{-10{,}300}{T_{PEN}}\right)$
Anode specific resistivity/Ω m	$\frac{95.0\times10^6}{T_{PEN}} \exp\left(\frac{-1150}{T_{PEN}}\right)$
Operating conditions	
Fuel utilization/%	85
Average current density/A m^{-2}	3000
Air excess ratio	7
Air feed	21% O_2, 79% N_2
Fuel feed	Steam/carbon > 2, 30% pre-reforming
Cells outlet pressure/Pa	101,325
Fuel inlet temperature/°C	900
Air inlet temperature/°C	900
PEN emissivity	0.8
Interconnector emissivity	0.3
Methane reforming data	
K coefficient	4274
m coefficient	1.0
n coefficient	0.0
Methane activation energy/J mol^{-1}	82,000
Activation polarization	
Activation energy of anode/kJ mol^{-1}	100
Activation energy of cathode/kJ mol^{-1}	117
Pre-exponential coefficient for anode/A m^{-2}	5.5×10^{-8}
Pre-exponential coefficient for cathode/A m^{-2}	7×10^{-8}
m coefficient	1.0
Diffusion polarization	
Pore diameter of anode/m	1×10^{-6}
Pore diameter of cathode/m	1×10^{-6}
Porosity of cathode /%	50
Porosity of anode /%	50
Tortuosity of cathode	3.0
Tortuosity of cathode	3.0
WGS reaction	
KWGS (mol s^{-1} m^{-2} Pa^{-1})	0.01

change ($J_{Final} - J_{Initial} > 0$), the cell starts with a given low fuel utilization and reaches a higher value for the new steady state operation. In a negative load change ($J_{Final} - J_{Initial} > 0$), the cell starts with a given high fuel utilization and reaches a lower value for the new steady state operation.

With regard to the first strategy, an example of the cell transient response is presented in Fig. 2 (Case 1). For this example, the initial average current density, fuel utilization, cell efficiency, and operating voltage (at $t < 0$), respectively are, 5000 A m^{-2}, FU = 85%, η_{Cell} = =39.7% and V_{op} = 0.520 V. At t ≥ 0, the average current density

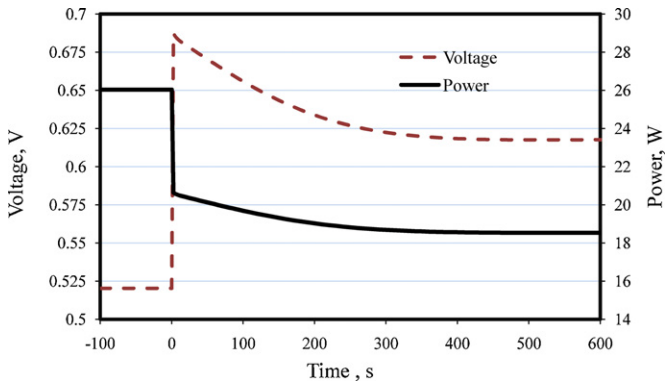

Fig. 2. Transient responses of cell voltage and power to step-load change from 5000 A m^{-2} to 3000 A m^{-2} (Case 1).

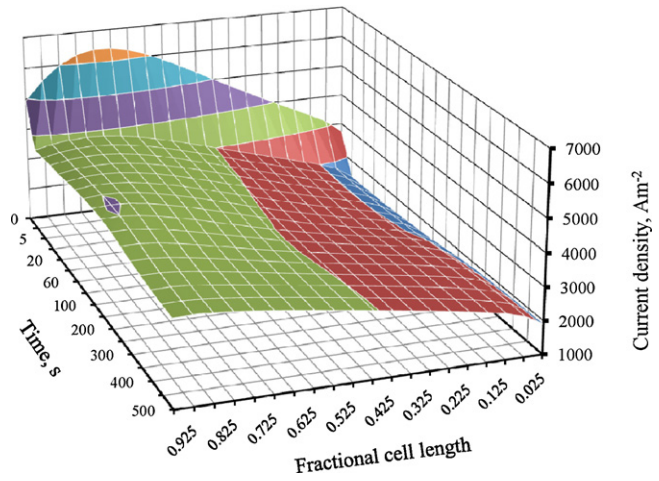

Fig. 3. Current density distribution along cell length as a function of time (Case 1).

is changed to 3000 A m^{-2}. As can be seen in Fig. 2, there is an overshooting of the cell voltage above the new steady state voltage. This overshoot has been observed by several authors [6,9,17–20] and it is correlated to the slow thermal response of the SOFC materials. The overshoot magnitude reported in the literature, however, is not the same and it is highly dependent on the applied control strategy, as well as the cell variable parameters.

The present model output results for η_{Cell}, FU, $V(t = +0)$ and $V(t \to \infty)$ are 28.3%, 51%, 0.687 and 0.618, respectively. The

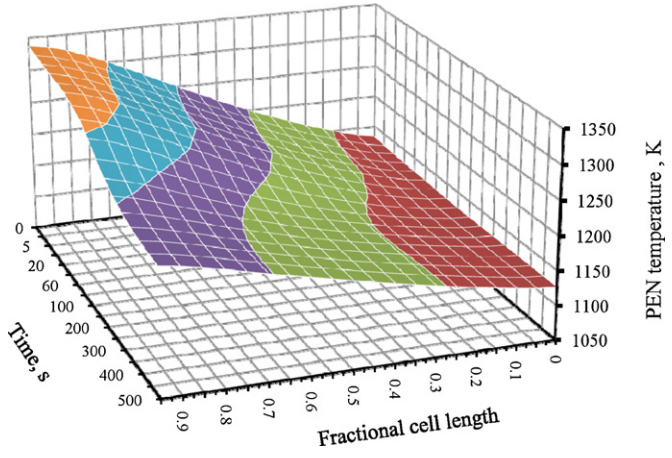

Fig. 4. PEN temperature distribution along cell length as a function of time (Case 1).

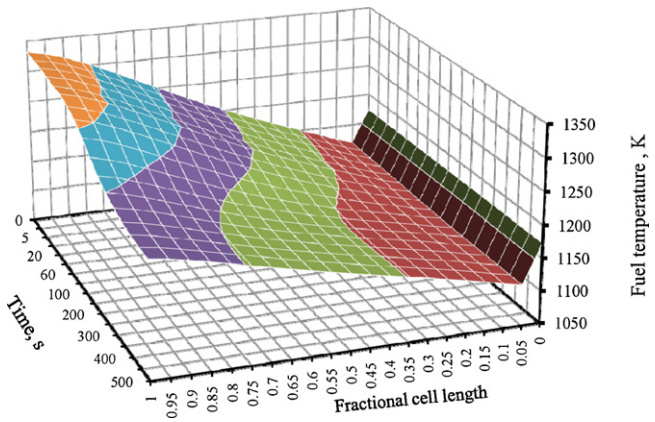

Fig. 5. Fuel flow temperature distribution along cell length as a function of time (Case 1).

relaxation times for recovering 90%, 95% and 99% of the dynamic voltage increase respectively are $\tau_{90\%} = 270$ s, $\tau_{95\%} = 315$ s and $\tau_{99\%} = 390$ s.

Figs. 3, 4 and 5 show the current density, the PEN (positive electrode–electrolyte–negative electrode) and fuel temperature distributions along the cell length, after the average current density step-change (or step-load change), until the new steady-state operation point. Due to the lower average current density and the lower FU in the SOFC new operation point, a smoother distribution for all three quantities can be observed in the new steady state condition. However, in spite of the cell voltage variation (Fig. 2), no jump in the PEN and fuel temperature distributions is observed.

In Fig. 6, the maximum and minimum temperatures of the cell, as well as the maximum cell temperature gradient, are shown. As can be seen, the maximum allowable local temperature gradient and the maximum allowable total temperature difference ($\Delta T_{total} = T_{max} - T_{min}$) along the cell are lower in the new steady state operation. However, high variation of the local temperature gradient and ΔT_{total} may cause damaging thermal stress within the SOFC components Therefore, although the above described strategy is an easy way to control an SOFC system, it is not an effective method and can cause harmful conditions during the SOFC operation points.

As a second example (Case 2), Fig. 7 shows the cell transient response to a new current density step-change i.e., 4000–3000 A m^{-2}. For this example, the model output results for η_{Cell}, FU, $V(t = +0)$ and $V(t \to \infty)$ are 28.3%, 51%, 0.64 and 0.618, respectively. The relaxation times for recovering 90%, 95% and 99% of the dynamic voltage increase respectively are $\tau_{90\%} = 300$ s,

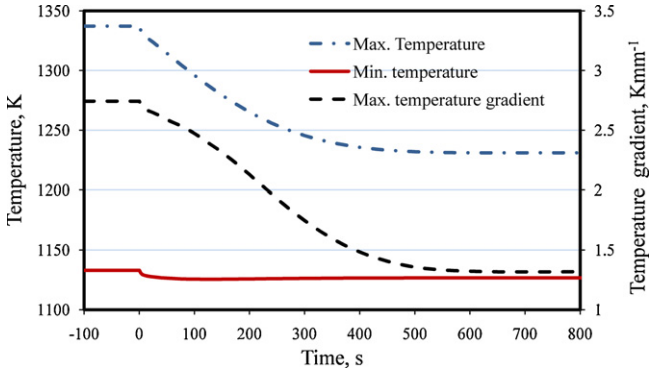

Fig. 6. Maximum and minimum temperatures and maximum cell temperature gradient as a function of time (Case 1).

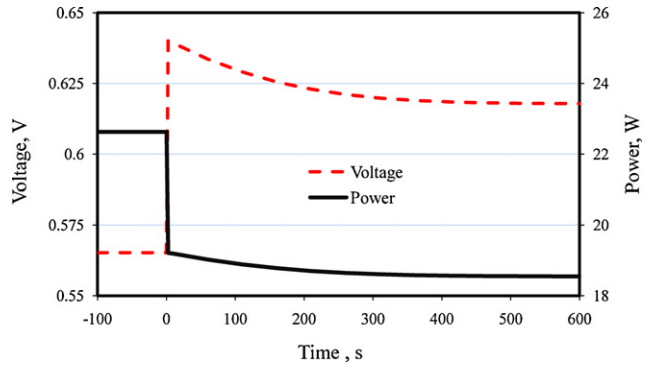

Fig. 7. Transient responses of cell voltage and power to step-load change from 4000 A m^{-2} to 3000 A m^{-2} (Case 2).

$\tau_{95\%} = 350$ s and $\tau_{99\%} = 430$ s.The presented results clearly show that the magnitude of the cell voltage overshoot is correlated with the magnitude of the average current density change (Case 1: $\Delta V = 0.069$ V and Case 2: $\Delta V = 0.022$ V), whereas, the relaxation time is almost independent of it.

In the second strategy, it was assumed that the FU parameter is constant during the cell transient operation. Therefore, after the step-load change ($t = +0$), a controller sets the fuel and air flow rates proportional to that new average current density, keeping the FU and AER constant. Therefore, in a positive load change, both fuel and air flow rates reach a higher value, and vice versa. In Fig. 8 (Case 3), an example of the cell dynamic response under this condition is shown. For this example, the initial average current density, fuel utilization, cell efficiency and operating voltage are 3000 A m^{-2} (at $t < 0$), FU = 85%, $\eta_{Cell} = 48.1\%$ and $V_{op} = 0.630$ V, respectively. At $t \geq 0$, the average current density is changed to 5000 A m^{-2}. As can be seen in Fig. 8, there is an undershooting of the cell voltage below the new steady state voltage. However, the magnitude of this undershoot is lower than the overshoot magnitude, which is observed in Fig. 2, whereas, the variation of the load change is the same, but in different directions. The model output results for $V(t = +0)$ and $V(t \to \infty)$, η_{Cell} are 0.50, 0.52 and 39.8%, respectively. The relaxation times for recovering 90%, 95% and 99% of the dynamic voltage drop respectively are, $\tau_{90\%} = 130$ s, $\tau_{95\%} = 155$ s and $\tau_{99\%} = 190$ s. The new relaxation data are almost halved, compared to the previous results.

In Fig. 9, the maximum and minimum temperatures of the cell as well as the maximum cell temperature gradient for the above example are shown. In comparison to the curves presented in Fig. 6, both maximum allowable local temperature gradient and maximum cell temperature experience a lower change during the transient operation time.

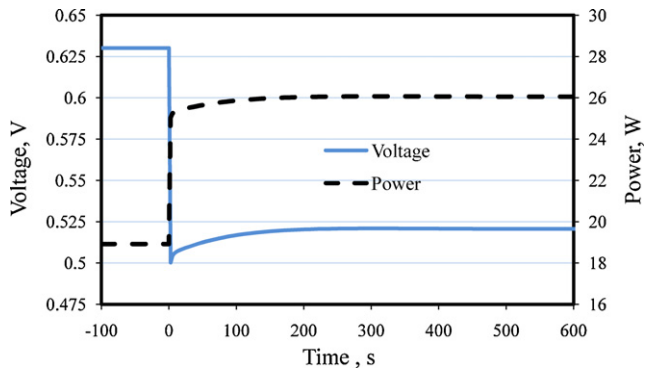

Fig. 8. Transient responses of cell voltage and power to step-load change from 3000 A m^{-2} to 5000 A m^{-2} (Case 3).

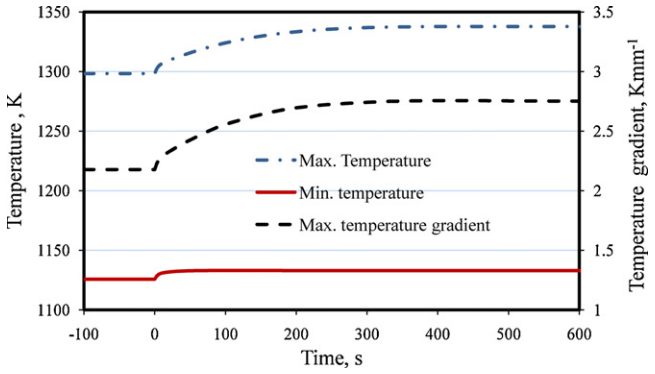

Fig. 9. Maximum and minimum temperatures and maximum cell temperature gradient as a function of time (Case 3).

It can be concluded that in the second strategy, the cell response is faster and the presented strategy can be effectively used to control an SOFC operation during a load change.

Finally, it is worth noting that the developed dynamic model shows the same general response and trends as the previous literature models [6,9,21]. The obtained relaxation times are also almost similar to those published for the planar SOFC cell [6,9,10,15].

4.2. Transient response to an inlet flow temperature change

The cell performance is highly dependent on its inlet flow temperatures. As a result, in a steady state operation point, the fuel and air temperatures to a stack are usually constant. However, in some cases, i.e., due to the failure of the system components, such as reformer, considerable changes in the inlet flow temperatures can occur.

In this section, the transient behaviour of a planar SOFC under an inlet flow temperature change is investigated (Case 4). Therefore, it is assumed that the inlet air and fuel temperatures decrease about 50 K from their initial values, i.e., 1173 K. In the initial steady state operation, the cell average current density, FU, AER, are 3000 A m^{-2}, 85%, 7, respectively. These values are kept constant during the simulation. The cell initial efficiency and voltage, respectively, are 48.1% and 0.63.

Fig. 10 shows the current density distribution along the cell length as a function of time. In comparison to Fig. 3, the current density variation is smoother here. The cell voltage and power versus time are shown in Fig. 11. As can be seen, these parameters

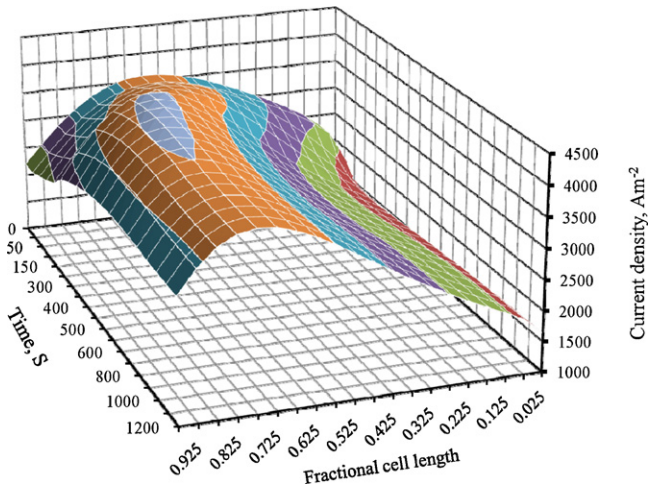

Fig. 10. Current density distribution along cell length as a function of time (Case 4).

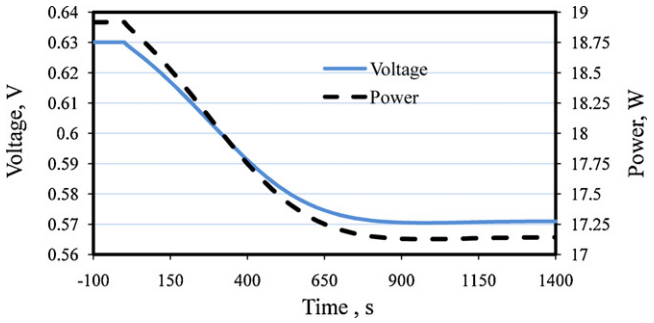

Fig. 11. Transient responses of cell voltage and power to inlet flow temperatures change from 1173 K to 1123 K (Case 4).

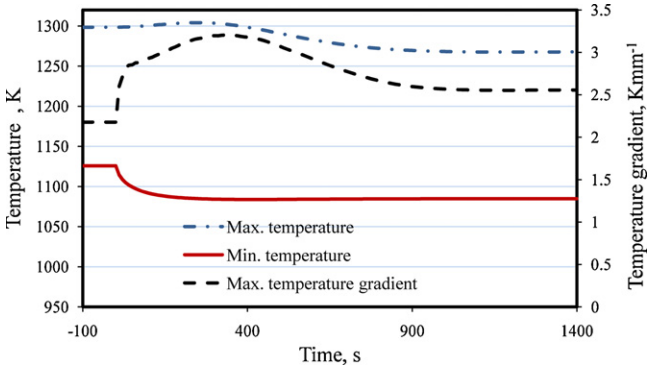

Fig. 12. Maximum and minimum temperatures and maximum cell temperature gradient as a function of time (Case 4).

gradually change over time, without any jump. The model output results for $V(t \to \infty)$ and η_{Cell} are 0.57 and 43.6%, respectively. The relaxation time for recovering 90%, 95% and 99% of the voltage drop, respectively, are $\tau_{90\%}$ = 590 s, $\tau_{95\%}$ = 685 s and $\tau_{99\%}$ = 800 s. These new relaxation data are at least two times higher, compared to the previous results. Therefore, it can be concluded that, for the case investigated, the cell response time to a flow inlet temperature change is slower than a step-load change. However, this is not generally correct as it is dependent on several parameters i.e., magnitude of change.

Maximum and minimum temperatures of the cell, as well as the maximum cell temperature gradient, are shown in Fig. 12. In comparison to the previous results, there is not any significant change in the maximum cell temperatures, whereas, there is an increase in the maximum cell temperature gradient curve and the cell temperature drop is more noticeable.

5. Conclusions

As an incremental step toward a more comprehensive understanding of the dynamic behaviour of planar DIR-SOFC systems, a previously developed steady state SOFC cell model was converted to a dynamic cell model. This dynamic model was employed here to explore the dynamic characteristics of a SOFC cell under several step-load and an inlet flow temperature changes. The step-load changes were investigated under two control strategies. In the first one, it was assumed that the fuel and air flow rates to the cell were constant during the cell transient operation. In the second strategy, however, the fuel and air flow rates were variable and their values were proportional to the cell new average current density, keeping the FU and AER constant. The results show that the relaxation time is strongly related to the thermal behaviour of the cell and the applied control strategy. However, it is almost independent of the load variation magnitude. It was observed that the cell

temperature and its gradient variations, as well as the relaxation time, were smaller in cases where the cell worked under a constant FU during the transition time. Therefore, the second strategy can be effectively used to control an SOFC operation during a load change. Results obtained from the simulation of the cell transient behaviour during an inlet flow temperature change also proved that for the case simulated, relaxation times were at least two times higher, compared to the previous results for the load changes.

Acknowledgements

The support of the Iran Renewable Energies Organization, Fuel cell Steering Committee for this work is acknowledged.

References

[1] S. Campanari, P. Iora, Fuel Cells 5 (2005) 34–51.
[2] J.R. Fergusen, J.M. Fiard, R. Herbin, Journal of Power Sources 58 (1996) 109–122.
[3] M. Iwata, T. Hikosaka, M. Morita, et al., Solid State Ionics 132 (2000) 297–308.
[4] F.P. Nagel, T.J. Schildhauer, S.M.A. Biollaz, A. Wokaun, Journal of Power Sources 184 (2008) 143–164.
[5] A. Pramuanjaroenkij, S. Kaka, X.Y. Zhou, International Journal of Hydrogen Energy 33 (2008) 2547–2565.
[6] E. Achenbach, Journal of Power Sources 57 (1995) 105–109.
[7] T. Ota, M. Koyama, C. Wen, K. Yamada, H. Takahashi, Journal of Power Sources 118 (2003) 430–439.
[8] K. Sedghisigarchi, A. Feliachi, IEEE Transactions on Energy Conversion 19 (2004) 423–428.
[9] P. Aguiar, C.S. Adjiman, N.P. Brandon, Journal of Power Sources 147 (2005) 136–147.
[10] Y. Kang, J. Li, G. Cao, H. Tu, J. Li, J. Yang, Journal of Power Sources 188 (2008) 170–176.
[11] M. Bavarian, M. Soroush, I.G. Kevrekidis, J.B. Benziger, Industrial and Engineering Chemistry Research 49 (2010) 7922–7950.
[12] D. Bhattacharyya, R. Rengaswamy, Industrial and Engineering Chemistry Research 48 (2009) 6068–6086.
[13] P. Kazempoor, V. Dorer, F. Ommi, Fuel Cells 10 (2010) 1074–1094.
[14] P. Kazempoor, V. Dorer, F. Ommi, International Journal of Hydrogen energy 34 (2009) 8630–8644.
[15] R.S. Gemmen, in: R. Bove, S. Ubertini (Eds.), Modeling Solid Oxide Fuel Cells: Methods, Procedures and Techniques, Springer, New York, 2008, pp. 269–323.
[16] R.J. Kee, P. Korada, K. Walters, M. Pavol, Journal of Power Sources 109 (2002) 148–159.
[17] R.S. Gemmen, C.D. Johnson, Journal of Power Sources 144 (2005) 152–164.
[18] Y. Mollayi Barzi, M. Ghassemi, M.H. Hamedi, Journal of Power Sources 192 (2009) 200–207.
[19] M. Molinelli, D. Larrain, N. Autissier, R. Ihringer, J. Sfeir, N. Badel, O. Bucheli, Journal of Power Sources 154 (2006) 394–403.
[20] D. Bhattacharyya, R. Rengaswamy, C. Finnerty, Chemical Engineering Science 64 (2009) 2158–2172.
[21] H. Xi, Dynamic modeling and control of planar SOFC power systems, PhD Thesis, The University of Michigan, 2007.